EPJ Web of Conferences **303**, 02004 (2024) https://doi.org/10.1051/epjconf/202430302004
MENU 2023

Recent results of Baryon electromagnetic form factors at BESIII

Lei Xia[*] for the BESIII Collaboration

[1]University of Science and Technology of China
State Key Laboratory of Particle Detection and Electronics

Abstract. Baryon Electromagnetic Form Factors are essential for testing ground state models of nucleon internal structures. At the BESIII experiment, a comprehensive study has been conducted on the electromagnetic form factors of various baryons. The electromagnetic form factor ratio of the nucleon (proton and neutron), denoted as $|G_E/G_M|$, has been determined with high precision. And the study at BESIII has explored the cross sections of various baryon pairs, including Λ, Λ_c, Σ, Ξ, Ω and Δ from their respective thresholds. In the study conducted at BESIII, threshold effects have been observed in some baryon pairs, enhancing our understanding of these baryon interactions.

1 Introduction

The mass of baryons, which constitutes a major component of the universe's mass, primarily arises from the strong force rather than the Higgs mechanism [1, 2]. This contrasts with many meson characteristics that transition from quantum electrodynamics (QED) to Quantum chromodynamics (QCD), illustrating a unique aspect of QCD in baryon properties.

Figure 1 illustrates the fundamental Feynman diagrams for electron-hadron elastic scattering and the annihilation of e^+e^- into a baryon pair. For spin 1/2 baryons, the hadronic vertex is depicted by a dynamic matrix,

$$\Gamma_\mu(p', p) = \gamma_\mu F_1(q^2) + \frac{i\sigma_{\mu\nu}q^\nu}{2m_B c}\kappa F_2(q^2), \tag{1}$$

where F_1 and F_2 are the so called Dirac and Pauli Form Factors (FFs) and m_B is the mass of the corresponding baryon.

Sachs Form Factors connect to charge, magnetization distribution, and crucial to test ground state for models of the nucleon internal structure.

$$G_E(q^2) = F_1(q^2) + \tau\kappa F_2(q^2), G_M(q^2) = F_1(q^2) + \kappa F_2(q^2) \tag{2}$$

where $\tau = \frac{q^2}{4m_B^2c^2}$, $\kappa = \frac{g-2}{2}$ and $g = \frac{\mu}{J}$.

The cross section for the process $e^+e^- \to B\bar{B}$ ($\sigma^{\text{Born}}_{e^+e^-\to B\bar{B}}$) is given by:

$$\sigma^{\text{Born}}_{e^+e^-\to B\bar{B}}(s) = \frac{4\pi\alpha^2\beta C}{3s}\left[|G_M(s)|^2 + \frac{2m_B^2c^4}{s}|G_E(s)|^2\right], \tag{3}$$

[*]e-mail: xial@ustc.edu.cn

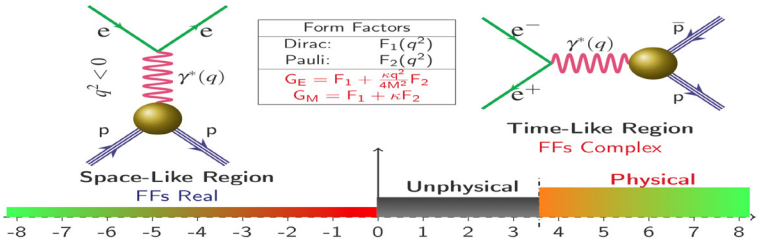

Figure 1. Lowest-order Feynman diagrams for elastic electron-baryon scattering $e^-B(p) \to e^-B(p)$, and for the annihilation process $e^+e^- \to p\bar{p}$ (right).

where α denotes the fine structure constant, $\beta = \sqrt{1 - 4m_B^2c^4/s}$ represents the baryon velocity, and C is the Coulomb enhancement factor [3]. Near the threshold, C leads the $\sigma^{\text{Born}}_{e^+e^-\to B\bar{B}}$ non-zero. The effective FF (G_{eff}) is derived under the assumption $|G_E| = |G_M|$:

$$|G_{\text{eff}}(s)| = \sqrt{\frac{\sigma^{\text{Born}}_{e^+e^-\to B\bar{B}}(s)}{\frac{4\pi\alpha^2\beta C}{3s}(1 + \frac{2m_B^2c^4}{s})}} = \sqrt{\frac{|G_M(s)|^2 + \frac{2m_B^2c^4}{s}|G_E(s)|^2}{1 + \frac{2m_B^2c^4}{s}}}. \tag{4}$$

Contemporary experiments, benefiting from enhanced statistical capabilities, have conducted differential $\sigma^{\text{Born}}_{e^+e^-\to B\bar{B}}$ measurements through angular analysis in the one-photon exchange approximation within the e^+e^- center-of-mass system. This approach enables the independent determination of the individual $|G_E|$ and $|G_M|$:

$$\frac{d\sigma_{p\bar{p}}(s)}{d\Omega} = \frac{\alpha^2\beta C}{4s}\left[|G_M(s)|^2(1 + \cos^2\theta) + \frac{4m_B^2c^4}{s}|G_E(s)|^2\sin^2\theta\right], \tag{5}$$

where θ is the polar angle of the emitted particles.

2 Nucleon Form Factors

2.1 Proton Form Factors

BESIII has conducted measurements of the $\sigma^{\text{Born}}_{e^+e^-\to p\bar{p}}$, $|G_{\text{eff}}|$, $|G_E/G_M|$, $|G_E|$ and $|G_M|$ of proton, utilizing both energy scan [4–6] and Initial State Radiation (ISR) techniques [7–9], and the results have illustrated in Figure 2. Our findings represent the highest level of precision achieved to date in the TL region. The use of both low-energy effective QCD [10] and perturbative QCD [11] has been validated for accurately describing the $\sigma^{\text{Born}}_{e^+e^-\to p\bar{p}}$:

$$\sigma^{\text{Born}}_{p\bar{p}}(s) = \begin{cases} \dfrac{e^{a_c}\pi^2\alpha^3}{s\left[1 - e^{-\frac{\pi\alpha_S(s)}{\beta(s)}}\right]\left[1 + \left(\frac{\sqrt{s}-2m_pc^2}{a_0}\right)^{a_1}\right]}, & \sqrt{s} \le 2.3094\ \text{GeV}, \\ \dfrac{2\pi\alpha^2\beta(s)C\left[2 + \left(\frac{2m_pc^2}{\sqrt{s}}\right)^2\right]e^{2a_2}}{3s^5\left[4\ln^2\left(\frac{\sqrt{s}}{a_0}\right) + \pi^2\right]^2}, & \sqrt{s} > 2.3094\ \text{GeV}, \end{cases} \tag{6}$$

with the strong coupling constant $\alpha(S)$, and we have consider strong interaction effects near the threshold. a_0 is the QCD parameter Λ_{QCD}, a_1 power-law dependence, related to the number of valence quarks. The result of the fitting is illustrated in Figure 2(a).

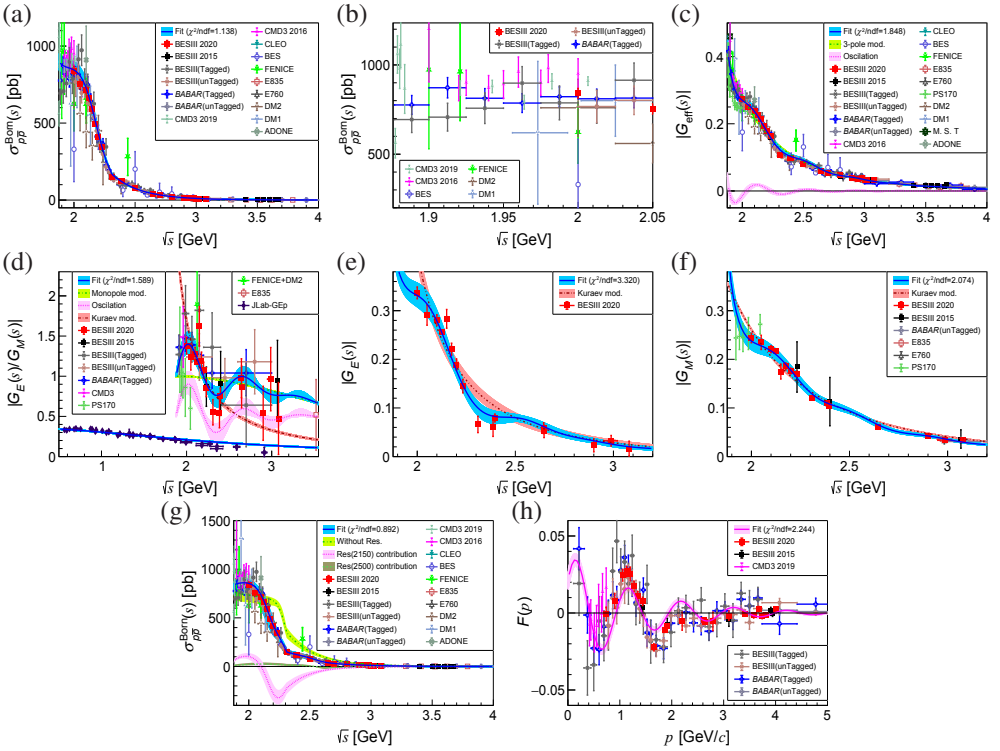

Figure 2. Results of (a) (b) $\sigma^{\rm Born}_{e^+e^-\to p\bar{p}}$, (c) $|G_{\rm eff}|$ (d) $|G_E/G_M|$ (e) $|G_E|$, and (f) $|G_M|$; (*g*) Fit $\sigma^{\rm Born}_{e^+e^-\to p\bar{p}}$ with two resonances; (h) Oscillation model.

An oscillatory behavior in the $|G_{\rm eff}|$ has been observed by the *BABAR* Collaboration [11] and subsequently confirmed by the BESIII Collaboration:

$$|G_{\rm eff}(s)| = \frac{\mathcal{A}}{(1+\frac{s}{m_a^2c^4})[1-\frac{s}{0.71\ {\rm GeV}^2}]^2} + b_0^{\rm osc}e^{-b_1^{\rm osc}p(s)}\cos(b_2^{\rm osc}p(s)+b_3^{\rm osc}), \tag{7}$$

and the result of the fitting is illustrated in Figure 2(c). The observed oscillation in $|G_{\rm eff}|$ is hypothesized to be due to the possibility of resonant structures around 2.15 GeV and 2.50 GeV (illustrated in Figure 2(g)), or alternatively, it might be explained by an oscillating function superimposed on a dipole parametrization (illustrated in Figure 2(h)).

For the $|G_E/G_M|$ of the proton, we have achieved a level of precision that is comparable to that in the space-like (SL) region. The revelation of periodic structures (illustrated in Figure 2(d)) in our data may be indicative of processes occurring at the subhadronic scale. Additionally, our analysis enables the extension of these findings to the individual $|G_E|$ (illustrated in Figure 2(e)) and $|G_M|$ (illustrated in Figure 2(f)), derived from the measured ratios $|G_E/G_M|$ and the $|G_{\rm eff}|$. Our implementation of a joint TL and SL fit has enhanced our understanding of the proton radius, as illustrated in Figure 2(d).

2.2 Neutron Form Factors

BESIII has performed measurements of the $\sigma^{\rm Born}_{e^+e^-\to n\bar{n}}$, $|G_{\rm eff}|$, $|G_E/G_M|$, $|G_E|$, and $|G_M|$ for the neutron from 2.00 to 3.08 GeV [12–14]. The results of these measurements are presented in Figure 3. Our findings indicate that the coupling of photons with protons ($\gamma-p$) is larger than

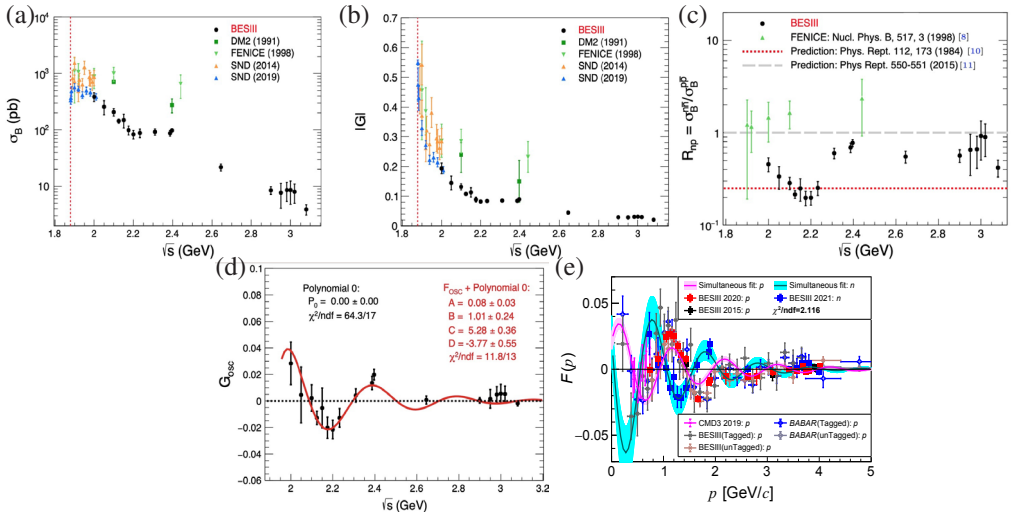

Figure 3. Results of (a) $\sigma^{\rm Born}_{e^+e^-\to n\bar{n}}$, (b) $|G_{\rm eff}|$ and (c) $\frac{\sigma^{\rm Born}_{e^+e^-\to n\bar{p}}}{\sigma^{\rm Born}_{e^+e^-\to n\bar{n}}}$; (d) Oscillation; (e) Simultaneously fitting the reduced $|G_{\rm eff}|$ for proton and neutron.

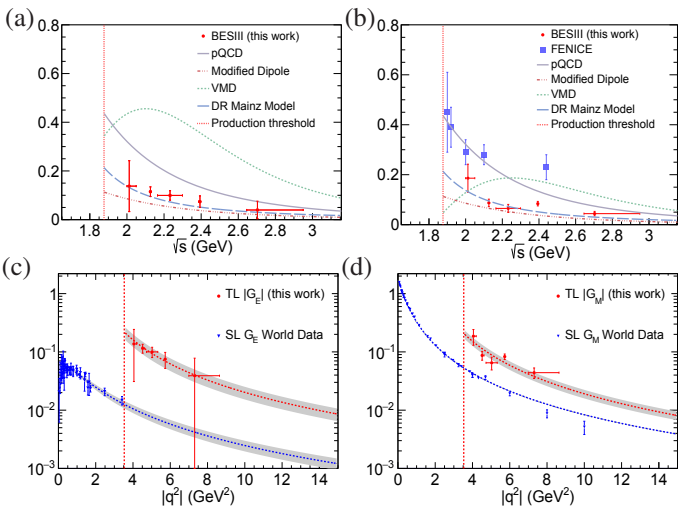

Figure 4. Results of Neutron FFs: (a) G_E; (b) G_M; (c) G_E compare with SL; (d) G_M compare with SL.

that with neutrons ($\gamma - n$), a result that aligns with theoretical predictions from Vector Meson Dominance (VMD) theory [15]. A similar oscillation effect is also discovered in the $|G_{\rm eff}|$ of the neutron, which have illustrated in Figure 3 (d) and (e). We performed a simultaneous fit of the reduced $|G_{\rm eff}|$ (illustrated in Figure 3 (f)), $|G_{\rm eff}|$, for both protons and neutrons, yielding a conjoint oscillation frequency for protons and neutrons of $b_2^{\rm osc} = (5.05^{+0.10}_{-0.09})$ (GeV/c)$^{-1}$, along with a phase difference relative to the proton of $\Delta b_3^{\rm osc} = (129^{+11}_{-10})^\circ$.

The G_E and G_M, have also been measured by the BESIII. Compared to the results from the FENICE experiment, our values for G_M are smaller by a factor of 2 to 3. We have compared our results with various theoretical models, including pQCD, a modified dipole model, VMD, and dispersion relations (DR). Among these, the dispersion relations model exhibits the best consistency with our findings, as illustrated in Figure 4.

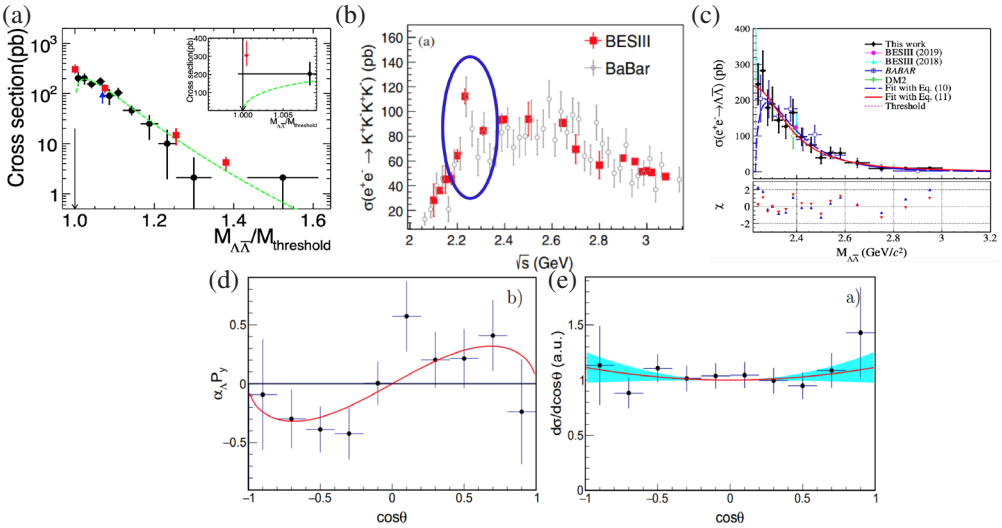

Figure 5. (a) $\sigma^{\rm Born}_{e^+e^-\to\Lambda\bar{\Lambda}}$ for energy scan technique; (b) $\sigma^{\rm Born}_{K^+K^-K^+K^-}$; (c) $\sigma^{\rm Born}_{\Lambda\bar{\Lambda}}$ for ISR technique; (d) (e) relative phase of Λ.

3 Hyperon Form Factors

3.1 Λ Form Factors

BESIII has performed measurements of the $\sigma^{\rm Born}_{e^+e^-\to\Lambda\bar{\Lambda}}$, employing both energy scan [16, 17] and Initial State Radiation (ISR) techniques [18]. The results of these measurements are presented in Figure 5. The non-zero $\sigma^{\rm Born}_{e^+e^-\to\Lambda\bar{\Lambda}}$ measured at 2.2324 GeV using the energy scan technique is $312 \pm 45^{+66}_{-36}$ pb. For the ISR technique, the measurements yield $245 \pm 56 \pm 14$ pb in the [2.231, 2.250] GeV range and $283^{+53}_{-55} \pm 15$ pb in the [2.25, 2.27] GeV range. These results are consistent with previous measurements in the field. A potential structure near the threshold has been identified in the $\sigma^{\rm Born}_{e^+e^-\to\Lambda\bar{\Lambda}}$ for the process $e^+e^- \to K^+K^-K^+K^-$. This structure is characterized by a resonance mass m_R of 2232 ± 3.5 MeV and an upper limit on the width Γ_R of less than 20 MeV [19]. BESIII has performed measurements of relative phase of Λ baryon, confirm the complex form of EMFFs: $|G_E/G_M| = 0.94 \pm 0.14 \pm 0.02$ and $\Delta\phi = 37^\circ \pm 12^\circ \pm 6^\circ$ [20].

3.2 Λ_c Form Factors

BESIII has achieved unprecedented precision in measuring $\sigma^{\rm Born}_{e^+e^-\to\Lambda_c\bar{\Lambda}_c}$ and $|G_E/G_M|$ [21–23], which illustrated in Figure 6. The plateau in $\sigma^{\rm Born}_{e^+e^-\to\Lambda_c\bar{\Lambda}_c}$ is confirmed up to 4.66 GeV, and no evidence for the decay process $Y(4630) \to \Lambda_c^+\bar{\Lambda}c^-$ is observed. In contrast to protons and neutrons, the Λc^+ $|G_{\rm eff}|$ spectrum does not exhibit an oscillation feature. However, an oscillation is discernible in the $|G_E/G_M|$ distribution of Λ_c^+, albeit with a frequency notably different from that observed in protons. Similar to protons, $|G_E/G_M|$ for Λ_c^+ tends to approach unity near the threshold.

3.3 Σ Form Factors

Investigations of the processes $e^+e^- \to \Sigma^+\bar{\Sigma}^-$, $e^+e^- \to \Sigma^-\bar{\Sigma}^+$, and $e^+e^- \to \Sigma^0\bar{\Sigma}^0$ revealed nonzero $\sigma^{\rm Born}_{\Sigma\bar{\Sigma}}$ near the threshold without significant enhancements [24–26], illustrated in

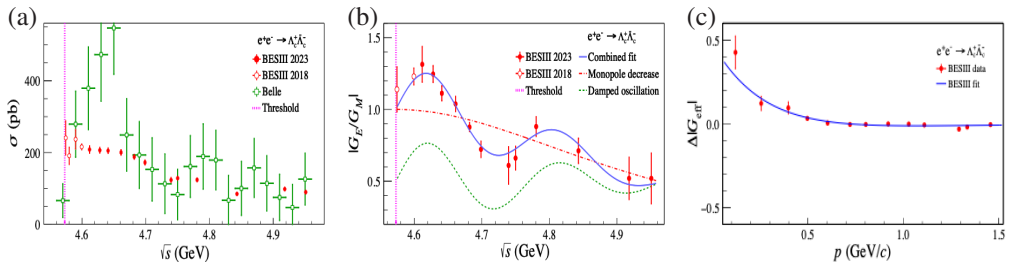

Figure 6. Results of Λ_c FFs: (a) $\sigma^{\rm Born}_{e^+e^-\to\Lambda\bar{\Lambda}}$; (b) $|G_E/G_M|$; (c) $\Delta|G_{\rm eff}|$.

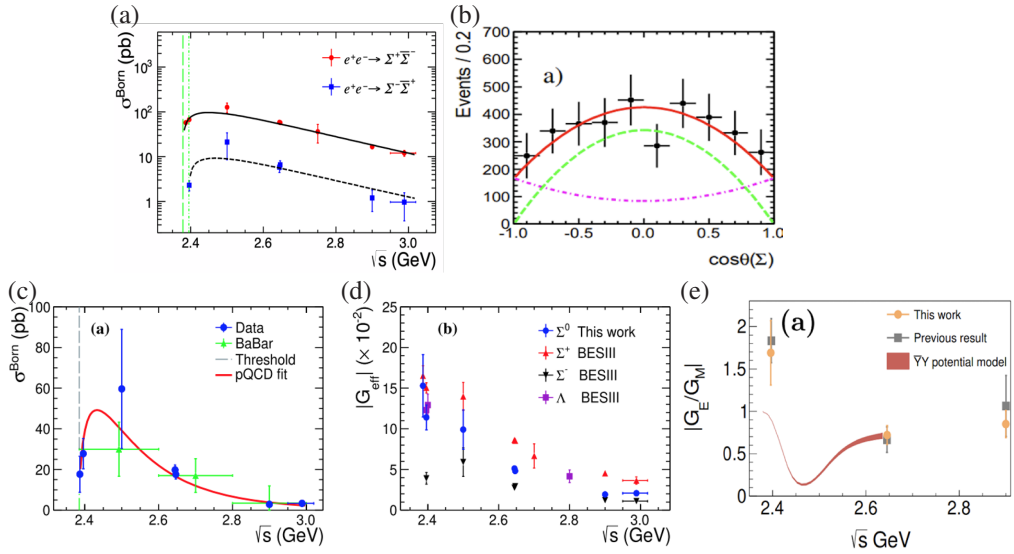

Figure 7. Results of Σ FFs: (a) $\sigma^{\rm Born}_{e^+e^-\to\Sigma^+\bar{\Sigma}^-}$ and $\sigma^{\rm Born}_{e^+e^-\to\Sigma^-\bar{\Sigma}^+}$; (b) $\cos\theta$ of Σ; (c) $\sigma^{\rm Born}_{e^+e^-\to\Sigma^0\bar{\Sigma}^0}$ and (d) $|G_{\rm eff}|$ of Σ^0; (e) confirm the complex form of EMFFs of Σ.

Figure 7. These measurements near the threshold show a deviation from point-like expectations, such as those for protons. $|G_E/G_M|$, of Σ^+ has been determined for the first time, with values of 1.83 ± 0.26 at 2.396 GeV, exceeding unity near the threshold and showing similarities to protons and lambda particles. $\frac{\sigma^{\rm Born}_{e^+e^-\to\Sigma^+\bar{\Sigma}^-}}{\sigma^{\rm Born}_{e^+e^-\to\Sigma^-\bar{\Sigma}^+}}$ was found to be 9.7 ± 1.3. An asymmetry in $\sigma^{\rm Born}_{\Sigma\bar{\Sigma}}$ among the Σ triplet is observed as $(9.7 \pm 1.3) : (3.3 \pm 0.7) : 1$, potentially indicating valence quark effects. The $|G_{\rm eff}|$ results provide experimental inputs for the $Y\bar{Y}$ potential model and contribute to our understanding of di-quark correlations, as discussed by [27]. BESIII has performed measurements of relative phase of Σ baryon [28], illustrated in Figure 7(e). Furthermore, the increasing trend of the relative phase suggests that the asymptotic threshold is yet to be reached, highlighting a new understanding in this area.

3.4 Ξ Form Factors

In the study of $e^+e^- \to \Xi\bar{\Xi}$ production near threshold, the BESIII collaboration conducted detailed investigations on $e^+e^- \to \Xi^-\bar{\Xi}^+$ [29, 31] and $e^+e^- \to \Xi^0\bar{\Xi}^0$ [30, 31], illustrated in Figure 8. Contrary to expectations, the study found no significant threshold enhancements

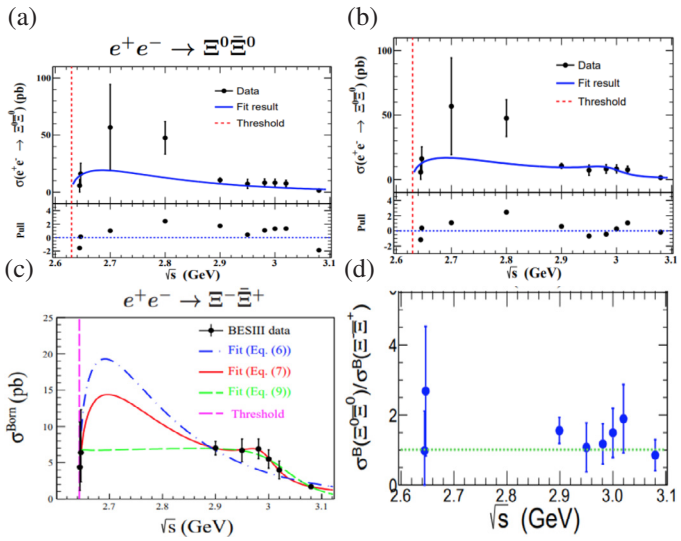

Figure 8. Results of Ξ FFs: (a)(b) $\sigma^{\rm Born}_{e^+e^-\to\Xi^0\bar{\Xi}^0}$; (c)(d) $\sigma^{\rm Born}_{e^+e^-\to\Xi^-\bar{\Xi}^+}$.

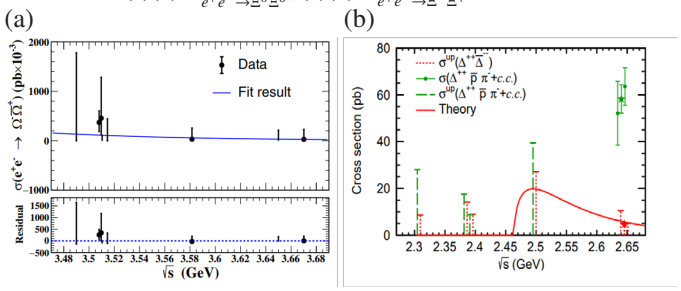

Figure 9. Results of (a) $\sigma^{\rm Born}_{e^+e^-\to\Omega^-\bar{\Omega}^+}$; (b) $\sigma^{\rm Born}_{e^+e^-\to\Delta^{++}\bar{\Delta}^{--}}$.

for either $\Xi^-\bar{\Xi}^+$ or $\Xi^0\bar{\Xi}^0$ production. Furthermore, the observed ratio of Born cross sections between $\Xi^0\bar{\Xi}^0$ and $\Xi^-\bar{\Xi}^+$ was consistent with isospin symmetry predictions, providing new insights into the nature of these processes.

3.5 Ω and Δ Form Factors

The study on $e^+e^- \to \Omega^-\bar{\Omega}^+$, with data spanning eight energy points from 3.49 to 3.67 GeV [32]. This study found no significant signals, but the upper limit of the $G_{\rm eff}$ was found to be consistent with perturbative QCD predictions (Figure 9(a)). The research of $e^+e^- \to \Delta^{++}\bar{\Delta}^{--}$ at five energy points from 2.3094 to 2.6464 GeV [33]. While no significant signal for $e^+e^- \to \Delta^{++}\bar{\Delta}^{--}$ was observed, a signal for $e^+e^- \to \Delta^{++}p\pi^-$ was detected, indicating new avenues of exploration in particle physics (Figure 9(b)).

4 Summary

Recent advancements in the field of EMFFs, gleaned from e^+e^- collider experiments using both energy scan and ISR methods, have yielded fruitful physics results. These findings challenge conventional parameterizations of EMFFs, as evidenced by observed threshold effects, oscillations in reduced form factors, and fluctuations in the $|G_E/G_M|$ ratio. The studies have successfully authenticated the relative phase and the predictions of perturbative QCD.

Notably, the periodic structure identified in EMFFs has been instrumental in causing the polarization of final-state baryons, marking a pivotal development in distinguishing various theoretical models. Furthermore, investigations into the asymptotic behavior of baryon EMFFs suggest that the theoretical asymptotic threshold is yet to be achieved, pointing to the need for continued research in this domain.

References

[1] K. Huang, Physics Today, **61**, 70-72 (2008).
[2] F. Wilczeck, *A Beautiful Question: Finding Nature's Deep Design* (Penguin Books, London, 2016).
[3] R. Baldini, S. Pacetti, A. Zallo and A. Zichichi, Eur. Phys. J. A **39**, 206 (2009).
[4] M. Ablikim *et al.* (BESIII Collaboration), Phys. Rev. D **91**, 112004 (2015).
[5] M. Ablikim *et al.* (BESIII Collaboration), Phys. Rev. Lett. **124**, 042001 (2020).
[6] L. Xia *et al.*, Symmertry **14**, 231 (2022).
[7] M. Ablikim *et al.* (BESIII Collaboration), Phys. Rev. D **99**, 092002 (2019).
[8] M. Ablikim *et al.* (BESIII Collaboration), Phys. Lett. B **817**, 136328 (2021).
[9] D. X. Lin *et al.*, Symmertry **14**, 91 (2022).
[10] O. P. Solovtsova *et al.*, Phys. Atom. Nucl. **73**, 1612 (2010).
[11] A. Bianconi *et al.*, Phys. Rev. Lett. **114**, 232301 (2015).
[12] M. Ablikim *et al.* (BESIII Collaboration), Nat. Phys. **17**, 1200 (2021).
[13] M. Ablikim *et al.* (BESIII Collaboration), Phys. Rev. Lett. **130**, 151905 (2023).
[14] P. Larin *et al.*, Symmertry **14**, 298 (2022).
[15] V. L. Chernyak *et al.*, Phys. Rept. **112**, 173 (1984).
[16] M. Ablikim *et al.* (BESIII Collaboration), Phys. Rev. D **97**, 032013 (2018).
[17] X. R. Zhou *et al.*, Symmertry **14**, 144 (2022).
[18] M. Ablikim *et al.* (BESIII Collaboration), Phys. Rev. D **107**, 072005 (2023).
[19] M. Ablikim *et al.* (BESIII Collaboration), Phys. Rev. D **100**, 032009 (2019).
[20] M. Ablikim *et al.* (BESIII Collaboration), Phys. Rev. Lett. **123**, 122003 (2019).
[21] M. Ablikim *et al.* (BESIII Collaboration), Phys. Rev. Lett. **120**, 132001 (2018).
[22] W. P. Wang *et al.*, Symmertry **14**, 5 (2022).
[23] M. Ablikim *et al.* (BESIII Collaboration), Phys. Rev. Lett. **131**, 191901 (2023).
[24] M. Ablikim *et al.* (BESIII Collaboration), Phys. Lett. B **814**, 136110 (2021).
[25] M. Irshad *et al.*, Symmertry **14**, 69 (2022).
[26] M. Ablikim *et al.* (BESIII Collaboration), Phys. Lett. B **831**, 137187 (2022).
[27] J. Haidenbauer *et al.*, Phys. Rev. D **103**, 014028 (2021).
[28] M. Ablikim *et al.* (BESIII Collaboration), arXiv:2307.15894.
[29] M. Ablikim *et al.* (BESIII Collaboration), Phys. Rev. D **103**, 012005 (2021).
[30] M. Ablikim *et al.* (BESIII Collaboration), Phys. Lett. B **820**, 136557 (2021).
[31] X. F. Wang *et al.*, Symmertry **14**, 65 (2022).
[32] M. Ablikim *et al.* (BESIII Collaboration), Phys. Rev. D **107**, 052003 (2023).
[33] M. Ablikim *et al.* (BESIII Collaboration), Phys. Rev. D **108**, 072010 (2023).